REPORT DOCUMENTATION PAGE

AFRL-SR-AR-TR-04-

0357

1. REPORT DATE (DD-MM-YYYY)	2. REPORT TYPE	3. DATES COVERED (From - To)
200504	Final Report	01 May 2000 - 31 Oct 2003

4. TITLE AND SUBTITLE
(DEPSCOR 00) A Fiber-Optic Sensor System for Total Lifetime Monitoring of Polymer Matrix Composites

5a. CONTRACT NUMBER

5b. GRANT NUMBER
F49620-00-1-0285

5c. PROGRAM ELEMENT NUMBER

6. AUTHOR(S)
Dr. Jon J. Kellar

5d. PROJECT NUMBER

5e. TASK NUMBER

5f. WORK UNIT NUMBER

7. PERFORMING ORGANIZATION NAME(S) AND ADDRESS(ES)
South Dakota School of Mines and Technology
501 E. St. Joseph Street
Rapid City SD 57701-3995

8. PERFORMING ORGANIZATION REPORT NUMBER

9. SPONSORING/MONITORING AGENCY NAME(S) AND ADDRESS(ES)
USAF/AFRL
AFOSR
801 N. Randolph Street
Arlington VA 22203

10. SPONSOR/MONITOR'S ACRONYM(S)
AFOSR

11. SPONSOR/MONITOR'S REPORT NUMBER(S)

12. DISTRIBUTION/AVAILABILITY STATEMENT
Distribution Statement A. Approved for public release; distribution is unlimited.

13. SUPPLEMENTARY NOTES

14. ABSTRACT
The most important progress has been made in the following two areas: strain sensitivity measurement and test geometry. The research on strain sensitivity measurement was focused on finding a system that did not have rapid stress relaxation. The transverse test geometry was shown to concentrate the transverse stress at the center of the sample. But the axial stress generated at the fiber-matrix interface was found to be greater than the transverse stress. Representative volume element analysis of the test geometry was also performed to investigate the effect of multiple fibers.

15. SUBJECT TERMS

20040715 118

16. SECURITY CLASSIFICATION OF:			17. LIMITATION OF ABSTRACT	18. NUMBER OF PAGES	19a. NAME OF RESPONSIBLE PERSON
a. REPORT	b. ABSTRACT	c. THIS PAGE			19b. TELEPHONE NUMBER (Include area code)
U	U	U	UU	32	

RECEIVED MAY 27 2004

1. COVER SHEET:

Principal Investigator: Dr. Jon J. Kellar,
Professor and Chairman

Institution: South Dakota School of Mines and Technology
Department of Materials and Metallurgical Engineering
501 E. St. Joseph Street
Rapid City, SD 57701-3995

Grant Number: F49620-00-1-0285

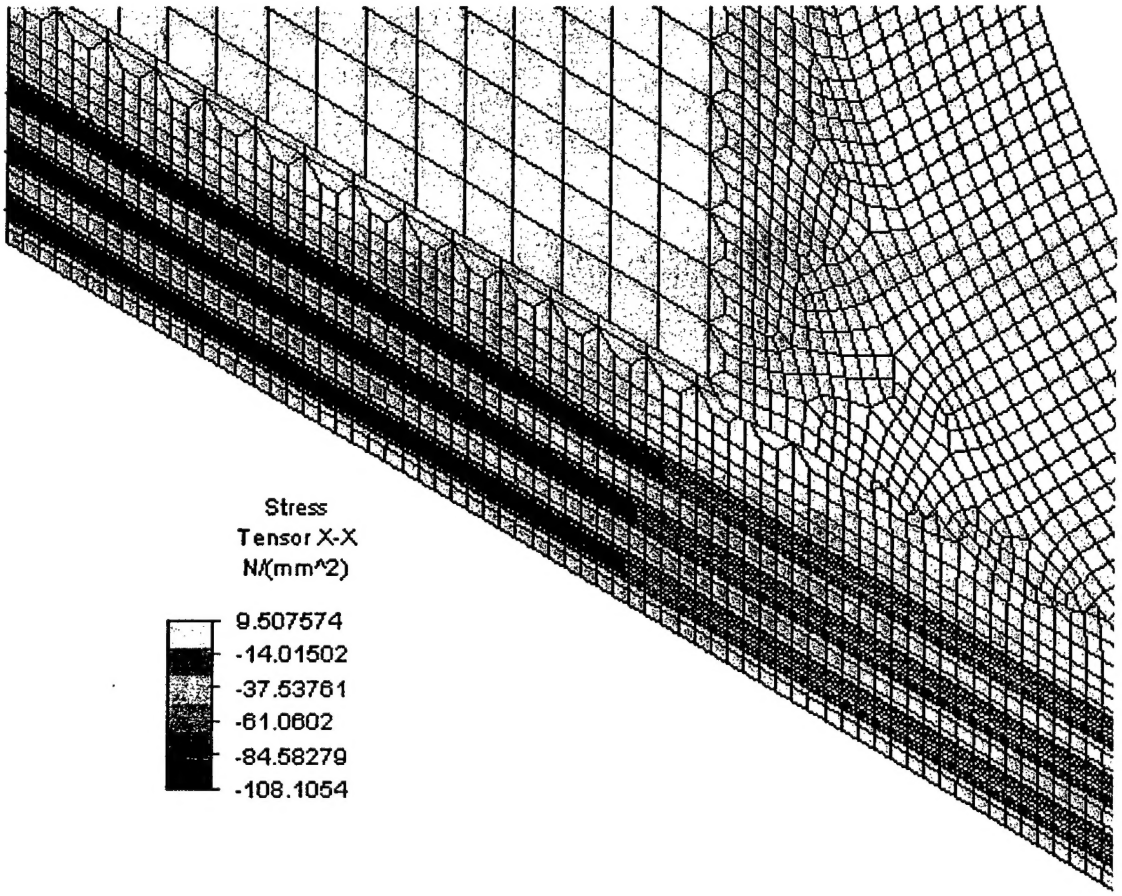

2. OBJECTIVES (have not deviated from the original):

The overall objective of this work is the development of a total lifetime, fiber-optic sensor system for polymer matrix composite materials. The sensor system to be developed will be able to monitor the polymer matrix composite, from initial processing, through use, and ultimately to failure. The sensor system will be based on inexpensive, 27 μm diameter, thin-clad glass fibers. The specific objectives of this proposal are to develop and calibrate both the chemical and mechanical sensing behavior of the fiber-optic sensor system in a model, unidirectional, single-ply laminate.

3. STATUS OF EFFORT

The project began in April, 2000. During the past year, progress was made in the following areas – strain sensitivity measurement and transverse testing. Strain sensitivity measurement research was primarily focused on finding a system that exhibited this effect and did not have rapid stress relaxation. Several systems were evaluated and the system EPON 828/EPI-CURE 3290 performed best; exhibiting a strain sensitivity of 2 wavenumber per percent strain shift in band position for the aliphatic overtone band located at approximately 5988 wavenumbers.

For transverse testing, finite element analysis of the test was continued. The transverse geometry was shown to concentrate the transverse stressing the center of the sample, but the axial stress generated at the fiber-matrix interface was greater than the transverse stress. Representative volume element (RVE) analyses of the transverse geometry were also performed to investigate the effect of multiple fibers on the system. In the first RVE analysis, the transverse geometry used in previous research on this grant was used, with relatively large fibers. In this RVE analysis, 1, 4 and 9-fiber models were compared. Generally, the differences seen between the stresses present at the fiber-matrix interface were relatively minor for the transverse, axial and shear stresses. The shear stress showed the greatest percentage difference of approximately 50%, but the value of the shear stress changed by only about 2.5 MPa, or 10% of the applied force. The axial and transverse forces were different by about the same stress amount as the shear stress, but this represented only about a 3-4% change in the value. Furthermore, all three RVE models showed very similar trends in the contribution of the different stresses to the von Mises stress. The axial stress was responsible for about 60% of the stress in the center of the specimen, the transverse about 38%. In the wings, the shear stresses became more important but the total force in the wings is much smaller than in the center of the specimen. Thus, the first model showed that the RVE approach is a good approach for examining the effect of multiple fibers and led to the second RVE model. For the second RVE model, the same geometry was used, but the fiber sizes were set such that 125 ~27 micron diameter fibers. The size and number of fibers were chosen to be equivalent to the size and number of fibers in the transverse test setup built during the previous research on this grant. Similar results, in terms of similarity of stress values and stress contribution to the von Mises stress were found for these new models as were found in the first RVE model. One important result from the second RVE model is that the axial stress value is now about 3 times the value in the first RVE, while the transverse stress is very similar to that of the first RVE. Thus, the axial stress is an even bigger problem for the transverse geometry when smaller fibers are simulated. Finally, the material properties of the constituents were changed to examine the effect of Young's modulus and Poisson's ratio on the axial and transverse stresses. Material properties that were closer to each other gave lower stresses and particularly reduced the axial stress. Altering the Young's modulus seemed to have a greater effect than altering the Poisson's ratio, although this conclusion may depend on the relative amount of change of the variables used.

4. ACCOMPLISHMENT/NEW FINDINGS

New findings have primarily been accomplished in two areas, strain sensitivity measurement and transverse testing. These new findings are described in the accompanying text.

A. Strain Sensitivity

Previously several polymer systems were investigated. A small subset of these, those containing relatively long aliphatic chains, were thought to be most likely to exhibit strain sensitivity. The first system examined was EPON 828 resin cured with EPI-CURE 3266 hardener. This hardener is composed primarily of long aliphatic chains capped with amine functional groups. Figure 1 shows a force-displacement curve for a thin film of this thermoset system. Testing was performed on a Minimat 2000 miniature materials tester. The force-displacement curve shows a very low level of maximum force (~1 N) at about 50% elongation. This behavior is more similar to an elastomer than to an epoxy. Therefore, the ability of the material to undergo creep or stress relaxation was of concern, because stress relaxation, in particular, would negate the desired band shift. Figure 2 shows a stress relaxation curve for an EPON 828/EPI-CURE 3266 thin film. Approximately 50% has relaxed within about 15 minutes. Therefore, no shifts of the aliphatic bands could be observed.

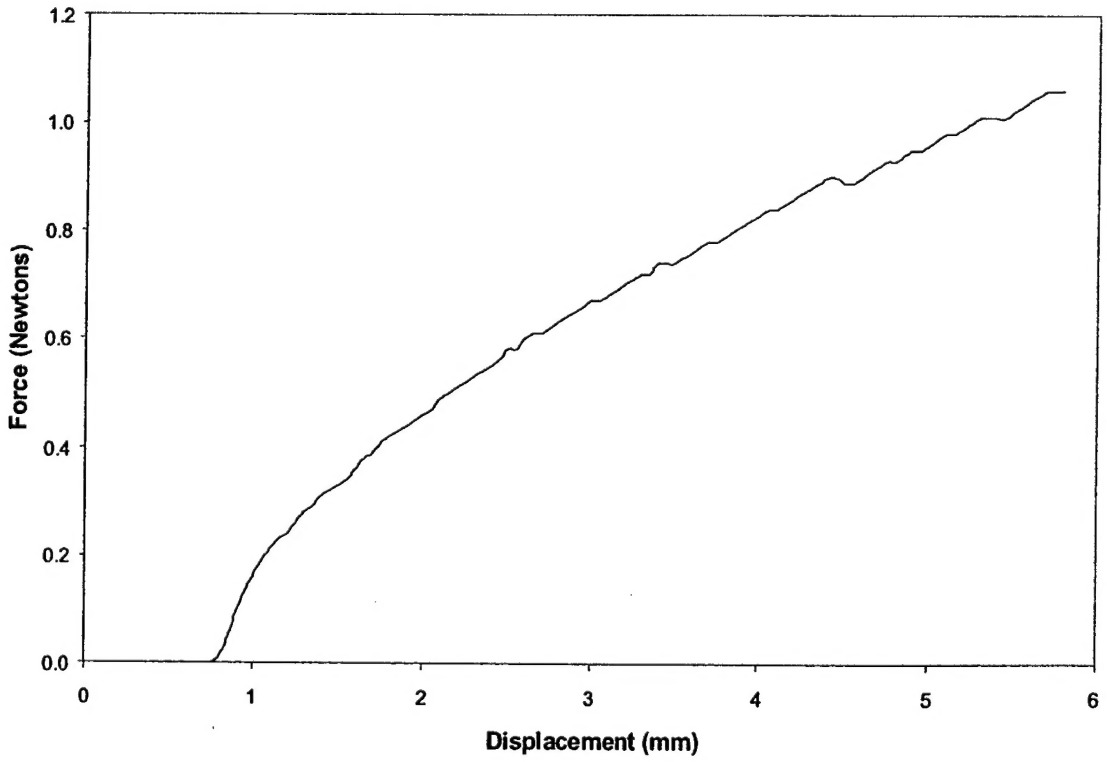

Figure 1. Force-displacement curve EPON 828/EPI-CURE 3266 polymer thin film.

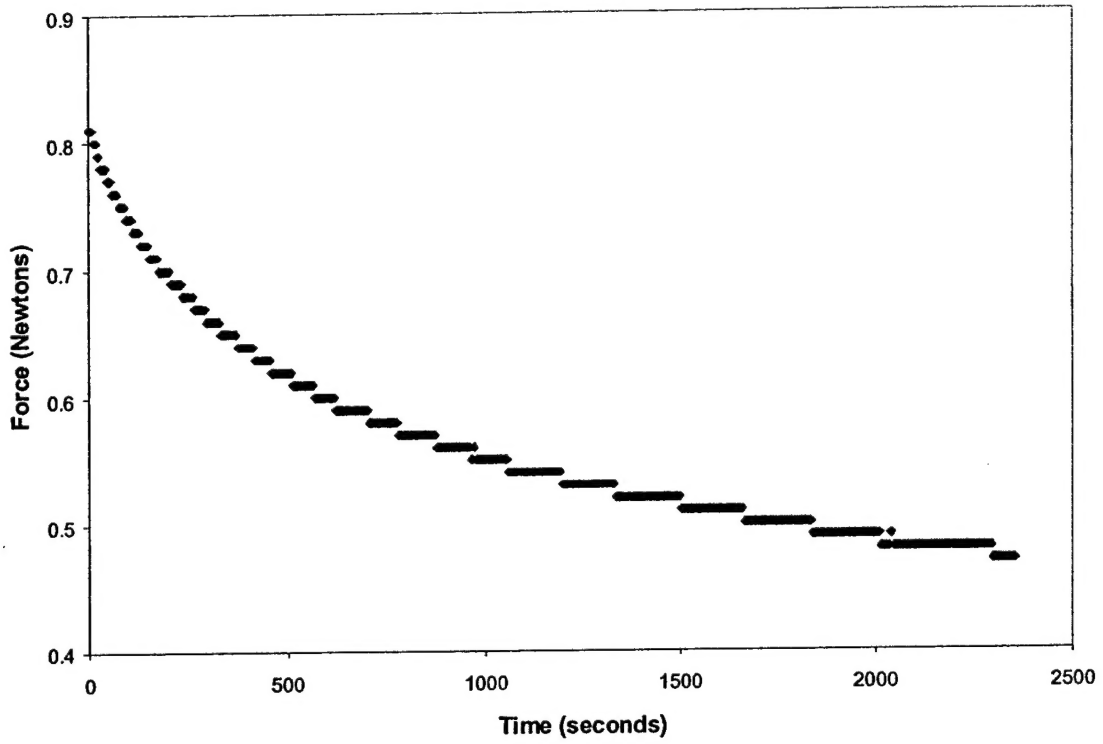

Figure 2. Stress relaxation curve for EPON 828/EPI-CURE 3266 polymer thin film.

As the initial system studied, EPON 828/EPI-CURE 3266, proved to have little or no band shift (rheo-optical) behavior, other systems were then examined. The main system studied in this regard was EPON 828/EPI-CURE 3290. This system is similar to the previous system, except the aliphatic chains are more branched. The force-displacement curve for a EPON 828/EPI-CURE 3290 thin film is shown in Figure 3. The maximum force is considerably greater than that observed for the EPON 828/EPI-CURE 3266 system (Figure 1) even though the film thicknesses were approximately equal. Furthermore, the EPON 828/EPI-CURE 3290 system displayed no observable stress relaxation. Thus, this system was chosen for further rheo-optical testing. Rheo-optical testing was performed with a PM-100 polymer modulator (Manning Applied Technology; purchased through a recent DURIP grant) placed in an FTS-6000 FT-IR spectrometer. A halogen near-IR source was used and a Peltier-cooled DTGS detector collected the IR light. The test was performed by gripping the polymer thin film at both ends approximately 15 mm apart. The film was stretched by turning a micrometer and following the micrometer signal until 1 micron movement occurred. At this point, the IR spectrum was collected. These spectra collected during testing were compared to spectra collected before and after testing to determine the band shift. Deconvolution of the spectra was performed to better define the band positions. Figure 4 shows a typical result from rheo-optical testing of EPON 828/EPI-CURE 3290. The primary aliphatic band examined was an aliphatic stretching overtone band located at approximately 5988 cm^{-1}. In addition, an aromatic stretching overtone band islocated at ~5758 cm^{-1}. From Figure 4, the aliphatic band shifted about 2 cm^{-1}, while the thin film was stretched

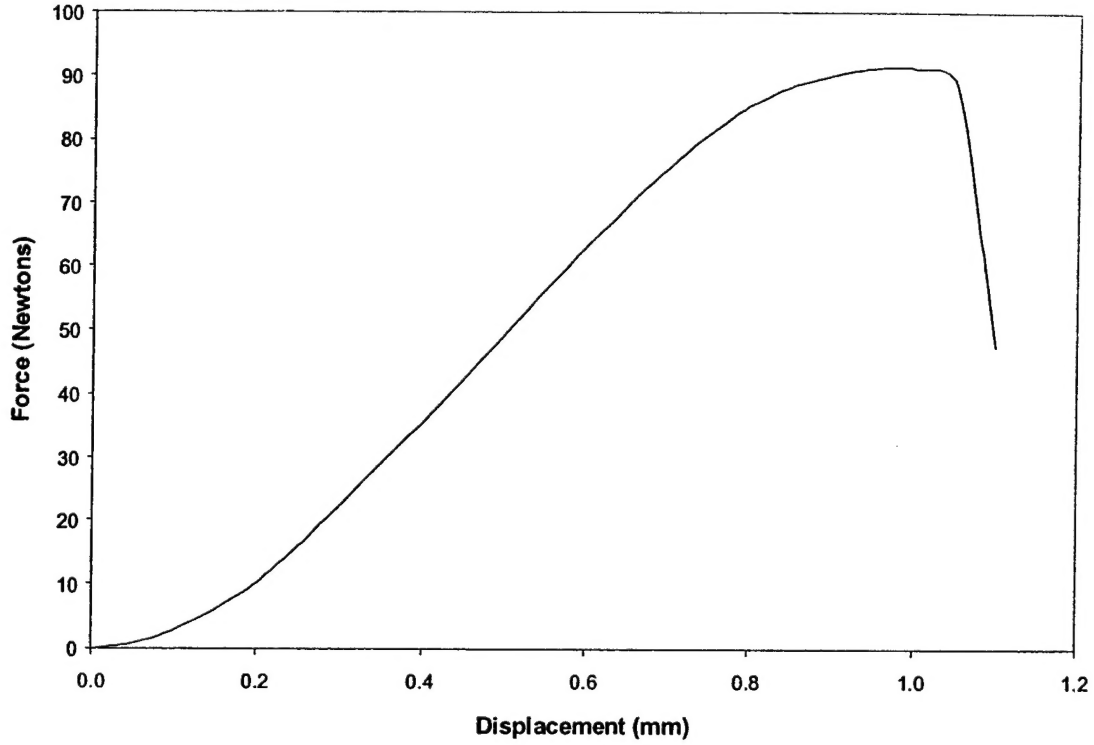

Figure 3. Force-displacement curve EPON 828/EPI-CURE 3290 polymer thin film.

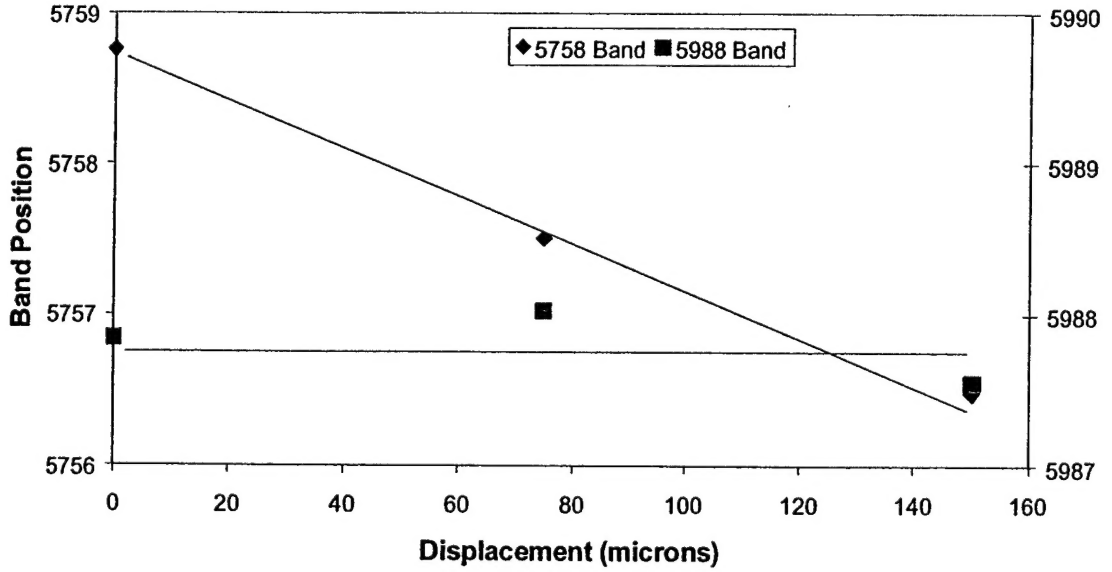

Figure 4. Rheo-optical data for EPON 828/EPI-CURE 3290 polymer thin film.

150 microns (about 1%). Concurrently, the aromatic band showed no appreciable shift, but did display a variation of about ±0.2 cm^{-1}. Thus, the aliphatic band sensitivity is about 0.1% strain or 100 microstrain units. This is somewhat less than found for strain only sensors such as Bragg gratings but still thought usable with an evanescent wave sensor such as that developed in this

research. This finding, when combined with previous findings showing the strain sensitivity of the fiber, shows that the evanescent wave sensor system utilized in this work has great potential for separating the strain behavior of the reinforcing fiber from the matrix in polymer matrix composites and allowing a better understanding of the stress transfer process in composite materials.

B. Transverse Testing

As most previous testing has been performed in a uniaxial tensile geometry, transverse tensile testing of composites containing the evanescent wave fiber-optic sensor system was investigated. Transverse testing was studied in three primary areas, test geometry, representative volume elements and specimen manufacture. Figure 5 shows the standard geometry for transverse testing. Transverse testing has been applied for many years in welding applications. Its use for polymer matrix composite material has been pioneered by Bechel et al. at the Wright-Patterson Air Force Research Labs. The primary purpose of this test is to allow load to be applied to a specimen in the direction transverse to the fiber direction. The wings are used to concentrate the load in the central portion of the specimen and allow more stress to be applied prior to failure.

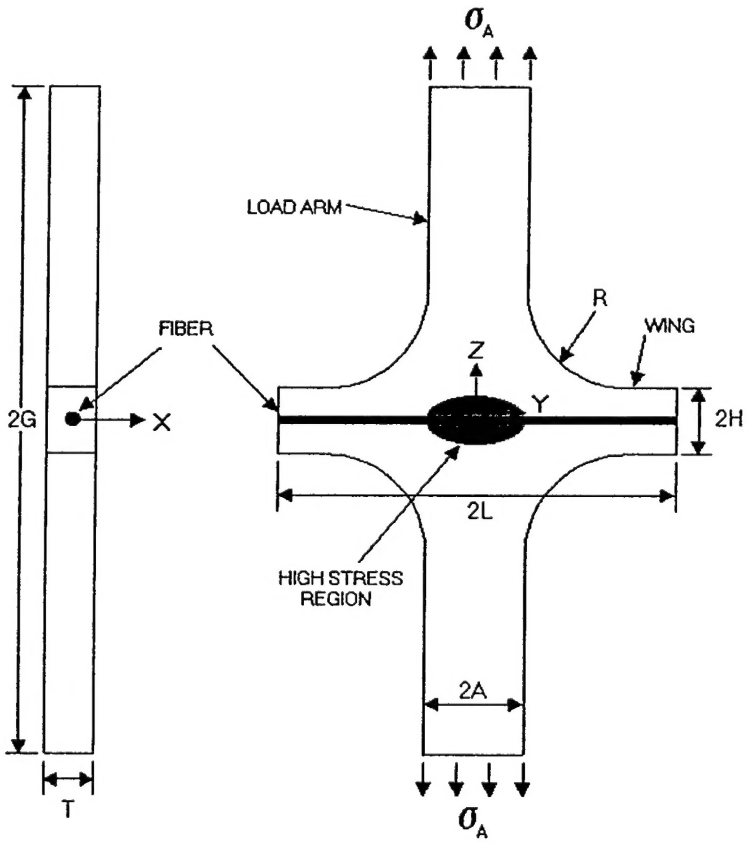

Figure 5. Transverse testing geometry.

Previously, the axial stress concentration along the fiber-matrix interface was examined for the geometry shown in Figure 5, and the effect of altering the wing height H in Figure 5 was also determined. In this year's report, the effect of wing width, L, and thickness, T has been determined. Also, representative volume element (RVE) models incorporating multiple fibers were studied.

Wing Width Comparison

During the previous year, the wing width (L) was analyzed. Table 1 contains the model parameters utilized.

Table 1: Dimensions Used for Wing Width Comparison

Parameter	A	H	L	T	R	G
Value	5.00 mm	1.16 mm	9.44 mm	1.00 mm	4.29 mm	7.50 mm
			10.00 mm			
			12.00 mm			
			14.00 mm			

3-D linear static stress analysis was performed using Algor analysis tools. Transverse stresses at the fiber-matrix interface are presented as stress concentration factors (SCFs) in Figure 6. The stress singularity at the free surface of the wing tip is c visible as the transverse SCF jump at the normalized distance of 1.0 in Figure 6.

The fiber axial stresses were taken at the fiber nodes just below the interface; and are presented as SCFs in Figure 7.

Effect of wing width on transverse stress Changing the wing width from 9.44 mm to 10 mm almost eliminated the singularity at the wing tip. Close inspection of the data indicated a slight jump in transverse stress at a wing width of 10 mm. Wing widths of 12 and 14 mm still produced a transverse stress increase at the free surface; however, the stress magnitudes were greatly reduced by these widths, however. Free surface stress and stress at the nearest interior node are given for comparison in Table 2.

Table 2: Comparison of Free Surface and Nearest Interior Node Transverse Stress

Wing Width (mm)	Interior Node Y location (mm)	Interior Node Stress (MPa)	Free Surface Stress (MPa)	Stress Increase (MPa)
9.44	9.293	0.137	0.441	0.304
10.00	9.860	0.0256	0.0831	0.0575
12.00	11.8462	131×10^{-6}	467×10^{-6}	336×10^{-6}

14.00	13.8462	0.856×10^{-6}	3.00×10^{-6}	2.144×10^{-6}

Thus, wider wings greatly reduce the stress singularity at the free surface, but do not completely eliminate this singularity. One could conclude that as the distance from the load arm increases, reliance on shear stresses to maintain equilibrium is reduced.

Effect of wing width on axial stress Wing width had little to no effect on the axial stress experienced by the fiber. Within practical limits, the axial stresses plotted in Figure 7 lie on top of one another. No reduction in axial stress was expected, because wider wings do little to reduce the overall Poisson effect.

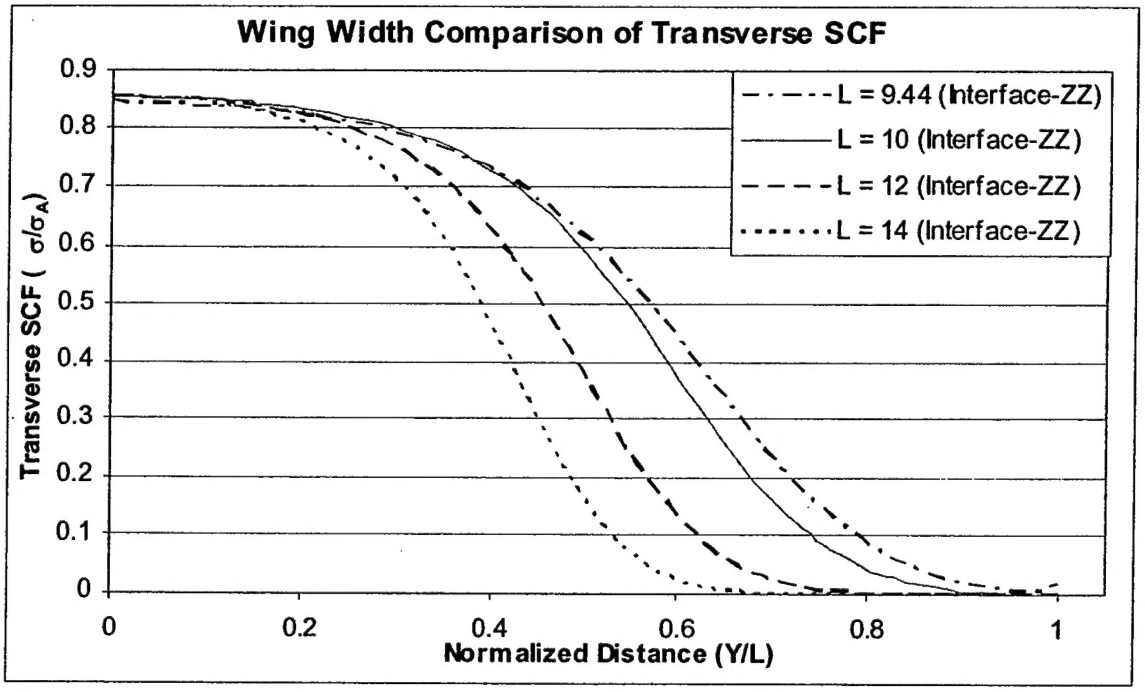

Figure 6. Transverse SCF for the cruciform test as a function of varying wing width.

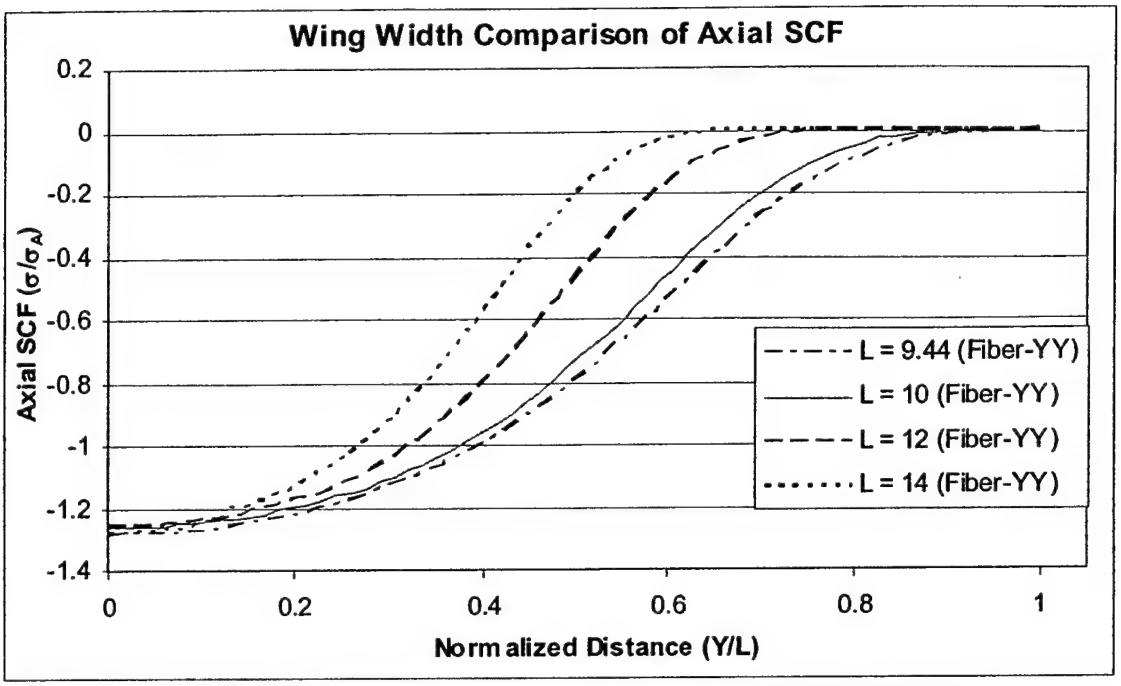

Figure 7. Axial SCF for the cruciform test as a function of varying wing width.

Specimen Thickness Comparison

In addition to the wing width, the effect of altering the specimen thickness was analyzed. The specimen geometry utilized is shown in Table 3. Stress concentration factors for the transverse and axial stress data are presented in Figures 8 and 9.

Table 3: Dimensions Used for Specimen Thickness Comparison

Parameter	A	H	L	T	R	G
Value	5.00 mm	1.16 mm	9.44 mm	0.125 mm	4.29 mm	7.50 mm
				1.00 mm		
				2.00 mm		
				4.00 mm		

Effect of specimen thickness on transverse stress There is a reduction in transverse stress of 1.02 MPa at the interface in the specimen center (Y = 0) as the thickness is increased from 0.125 mm to 2.00 mm. Though this is not a large reduction, the effect is undesirable because the purpose of this geometry is to focus as much transverse stress as possible toward the specimen center.

Effect of specimen thickness on axial stress Axial stress in the fiber increased in magnitude from -29.65 MPa to -32.67 MPa when going from 0.125 mm to 2.00 mm. Minimizing the axial compressive stress was one of the goals, so this is an adverse effect.

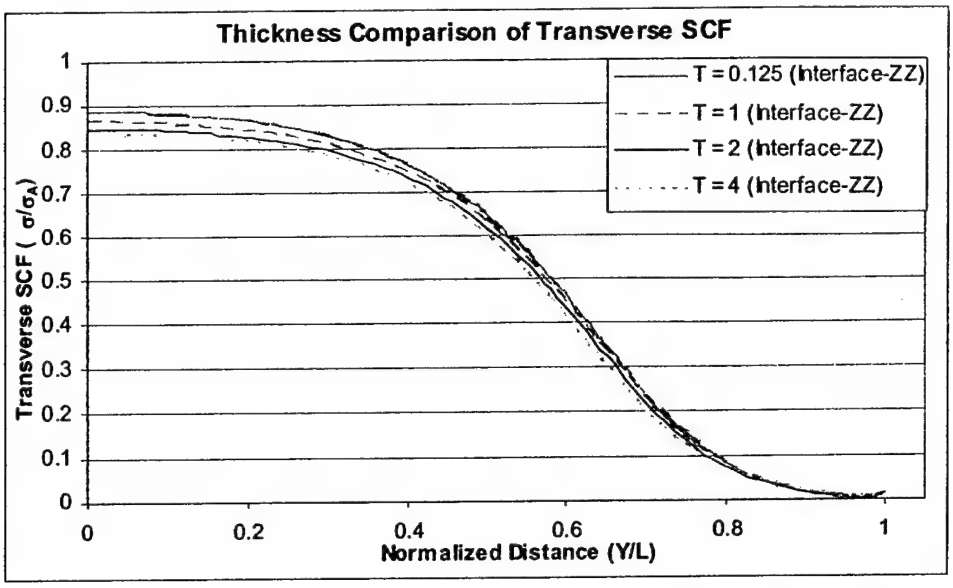

Figure 8. Transverse SCF for the cruciform test as a function of varying thickness.

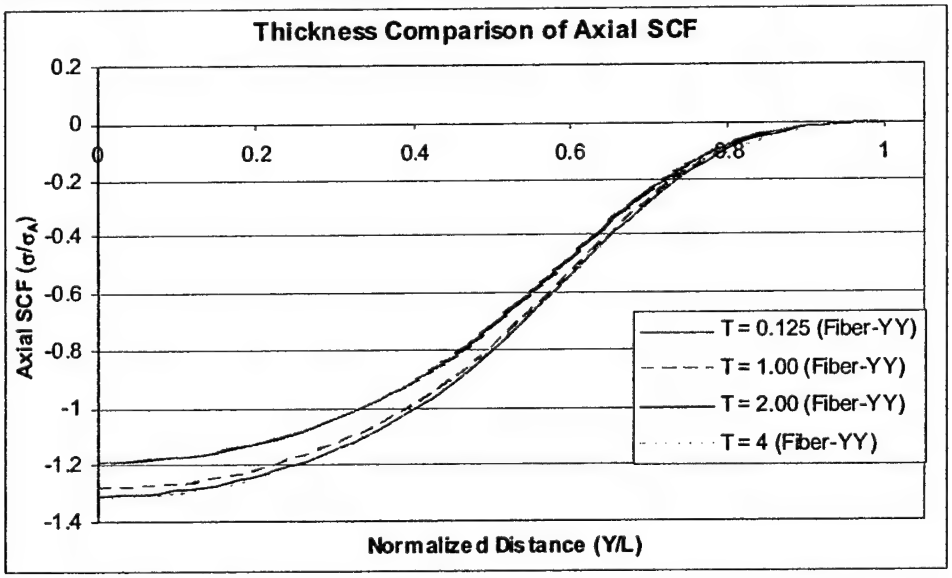

Figure 9. Axial SCFs for the cruciform test as a function of varying thickness.

Representative Volume Element Analysis

Two types of representative volume element (RVE) models were utilized. In the first type, 1, 4 and 9 fiber models were compared. The total fiber cross-sectional area was kept constant, so that the fibers in the 9-fiber model were 1/3 the radius of the 1-fiber model. The fiber size chosen in the 1, 4, 9 models was done for modeling convenience. In the second type, ¼, 1 and 4 fibers were used. In these models, the sizes were chosen to represent the cruciform specimen designed and used with the SDSM&T testing system.

First RVE 1-Fiber Model A total of 33256 8-node brick elements were used in the 1-fiber model. The largest aspect ratio was 3.1 occurring in the smaller fiber elements.

The highest transverse stresses (σ_{ZZ}) appear where the fiber and matrix meet in the specimen center (X = 0). The greatest axial stress (σ_{XX}) occurs just inside the fiber, though it remains close to constant through the entire fiber cross-section. The SCFs calculated from normal stresses and shear stresses are shown in Figures 9 and 10, respectively. Stress sensitivity factors (α) are plotted for all six stress components in Figure 11.

1-Fiber Stress concentration factors The general shape of the normal stress SCF graphs (Figure 9) is the same as that for the block fiber model; however, the magnitudes of both transverse and axial stresses are higher. A transverse (Z-Z) SCF greater than one is a good indication that stress is being concentrated at the specimen center. An axial (X-X) SCF of -1.9 at the interface is quite high (Figure 9), almost twice the applied stress. Axial stress seen at the fiber center is very high, yielding an SCF of -4.2. Interestingly, the lateral (Y-Y) SCF is positive indicating a tensile stress in the Y-Y direction at this location; opposite that for the block fiber. In addition, the shear SCFs have been investigated. For clarity, the Z-X SCF is calculated from shear stress in the X direction on the plane with normal in the Z. So, this is shearing the fiber/matrix interface in the direction of the fiber axis. One can see in Figure 10 that the shear stress increases dramatically to –0.20 SCF (-5.15 MPa), and then drops off as the wing tip is approached. This could be significant depending on the fiber/matrix interfacial shear strength. The X-Y and Y-Z are quite small and remain so through the entire specimen width.

1-Fiber Stress sensitivity factors As would be expected, transverse and axial stresses contribute most to the von Mises in the specimen's central region (Figure 11). But at a normalized distance of approximately 0.7, the Z-X shear becomes more influential than the transverse stress. At a normalized distance greater than 0.96, the Z-X shear becomes completely dominant until it drops at the free surface. As mentioned in the SCF section, this could be detrimental, particularly if residual stresses or de-bonding are already present in this area.

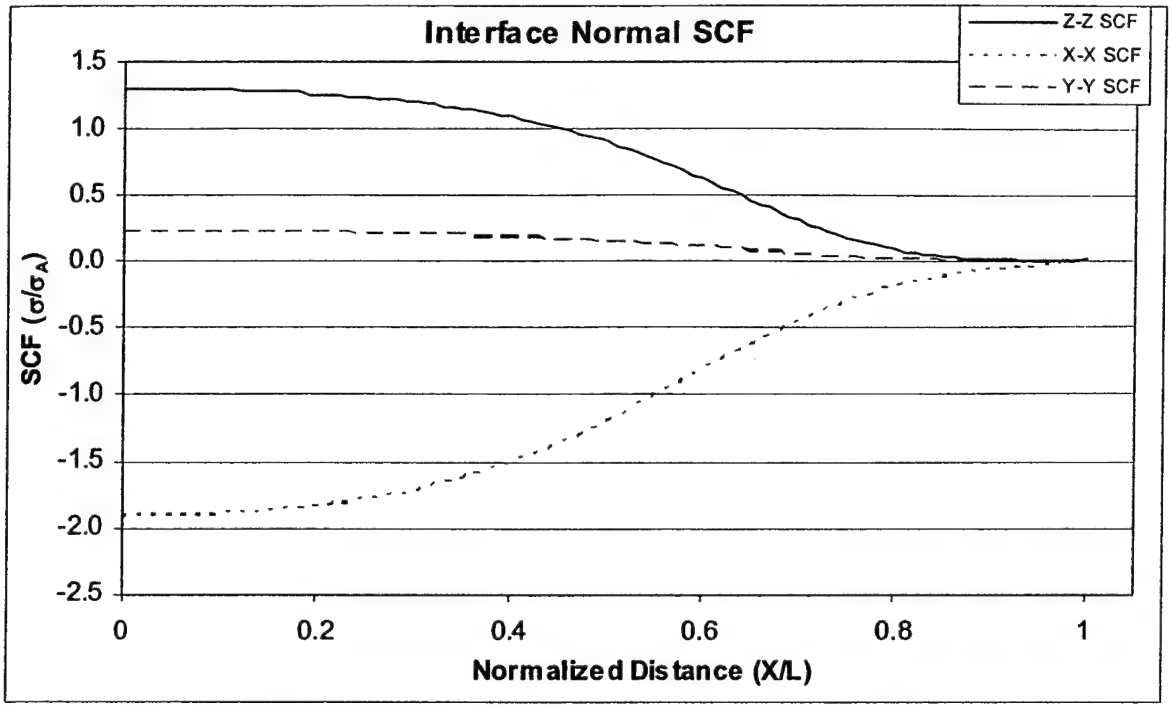

Figure 9. Normal stress concentration factors at the fiber/matrix interface.

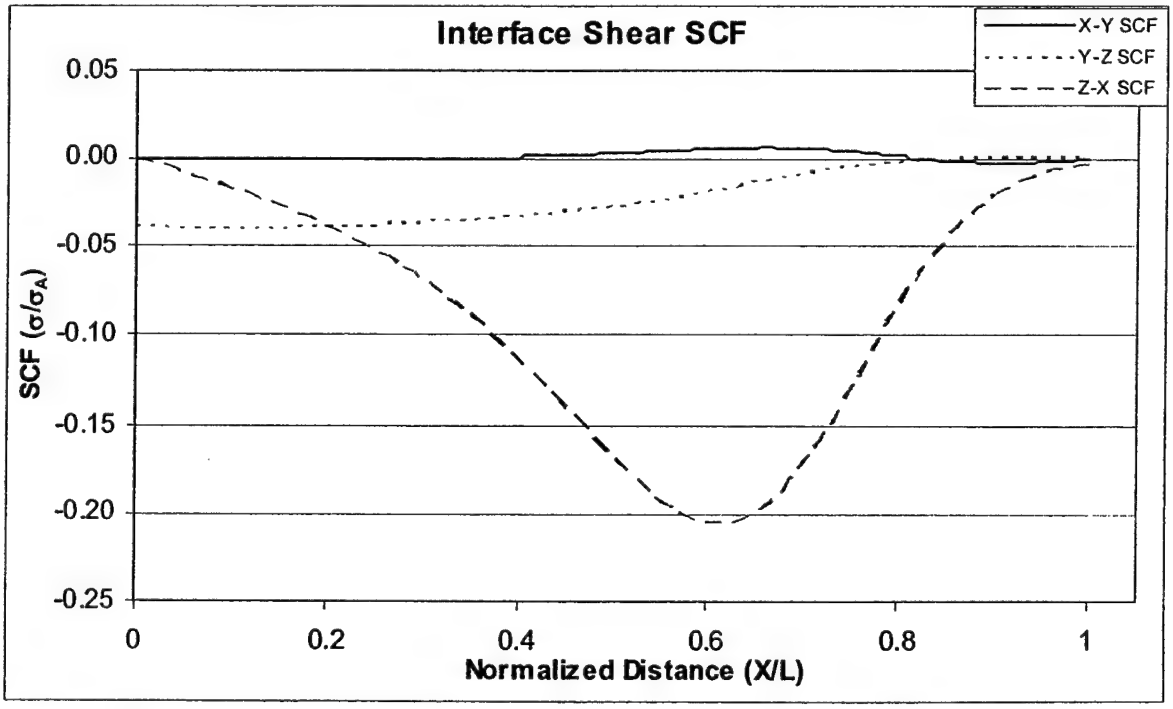

Figure 10. Shear stress concentration factors at the fiber/matrix interface.

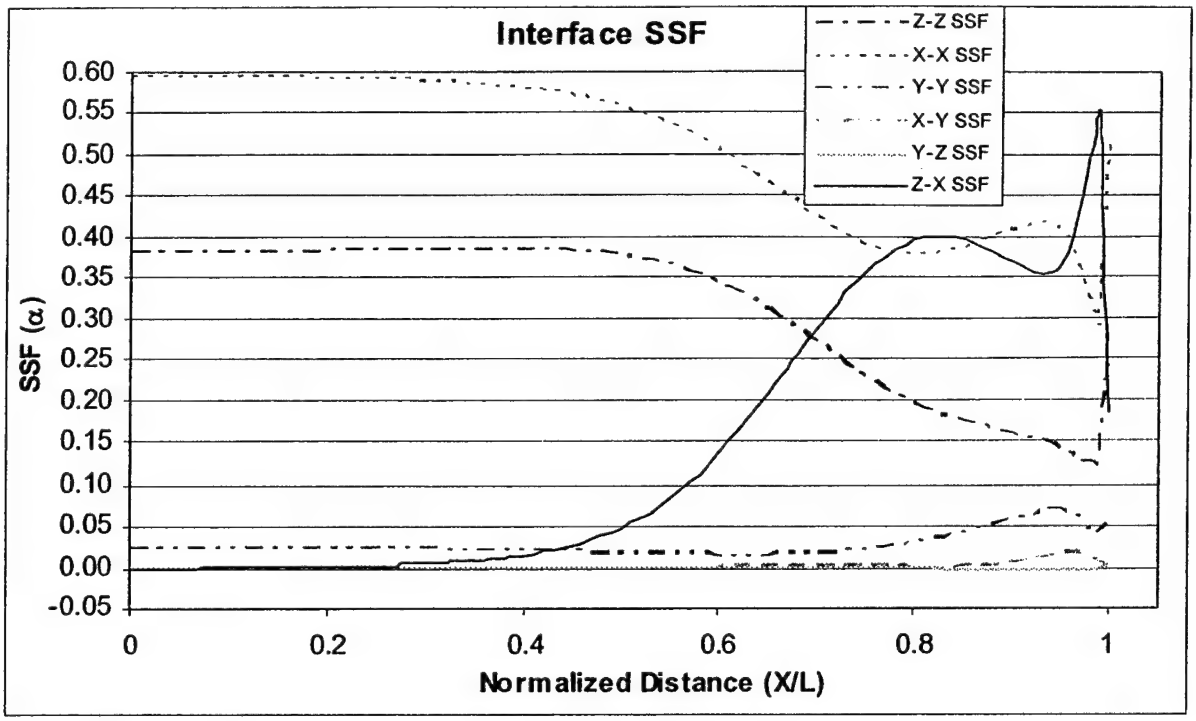

Figure 11. Stress sensitivity factors at the fiber/matrix interface.

First RVE 4-Fiber Model As the fibers get smaller, aspect ratios increase. For this model the highest aspect ratio of 5.1 occurred in the smaller fiber elements. 95,700 elements were used to create the complete model.

The highest transverse stresses occurring at X = 0. Likewise, the axial stress contours can be seen in Figure 12. Fiber 3 was chosen for comparison with the single fiber of the previous analysis. Normal and shear SCF from fiber 3 are plotted in Figures 13 and 14, respectively. Stress sensitivity factors for fiber 3 are presented in Figure 15.

4-Fiber Stress concentration factors All SCF curves are similar in shape to those of the single fiber model; magnitudes will be considered in a following section. In comparing transverse SCF for each fiber (Figure 12), a difference of 7% can be found between fiber 1 and 3. The axial SCF lie essentially on top of one another. Normal and shear SCF of fiber 3 (Figures 13 and 14) are very similar to those of the single fiber (Figures 10 and 11). The Z-X shear SCF has values of about half that for the single fiber, resulting in a maximum Z-X shear magnitude of -0.11 (-2.69 MPa).

4-Fiber Stress sensitivity factors Again, as would be expected, transverse and axial stresses contribute most to the von Mises in the specimen's central region (Figure 15). But, at a normalized distance of approximately 0.87, the Z-X shear becomes more influential than the transverse stress. At a normalized distance greater than 0.91, the Z-X shear becomes completely dominant until it drops near the free surface; shear stresses should drop completely to zero at the free surface, but as a consequence of modeling and averaging stresses to the nodes, the shear stresses do not go to zero.

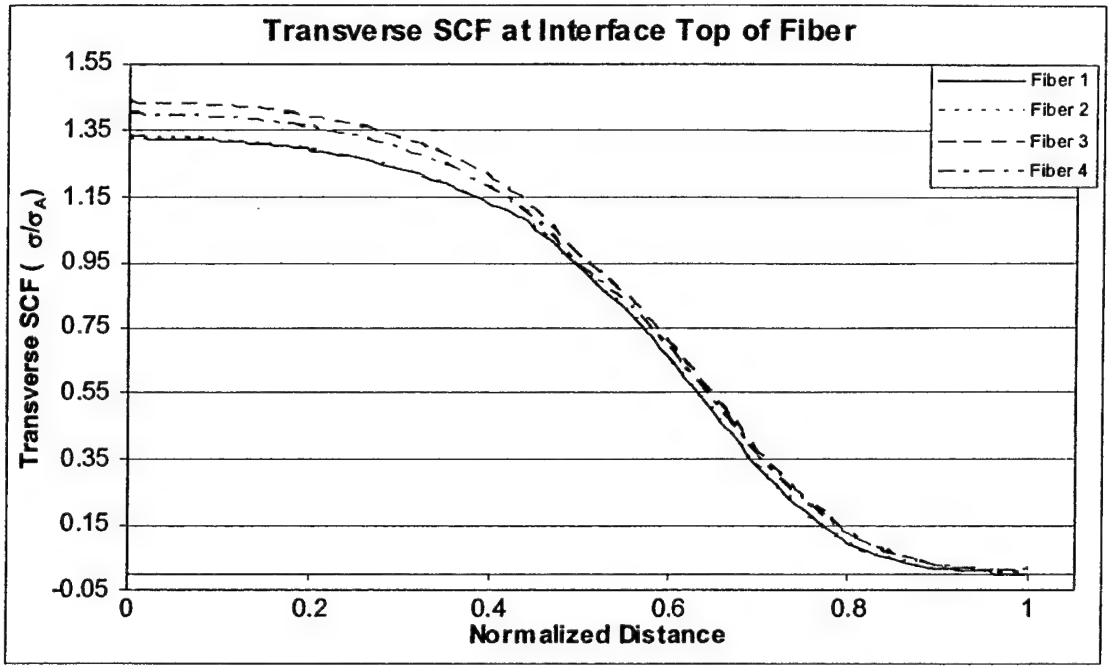

Figure 12. Comparison of interfacial transverse SCFs for the four fibers.

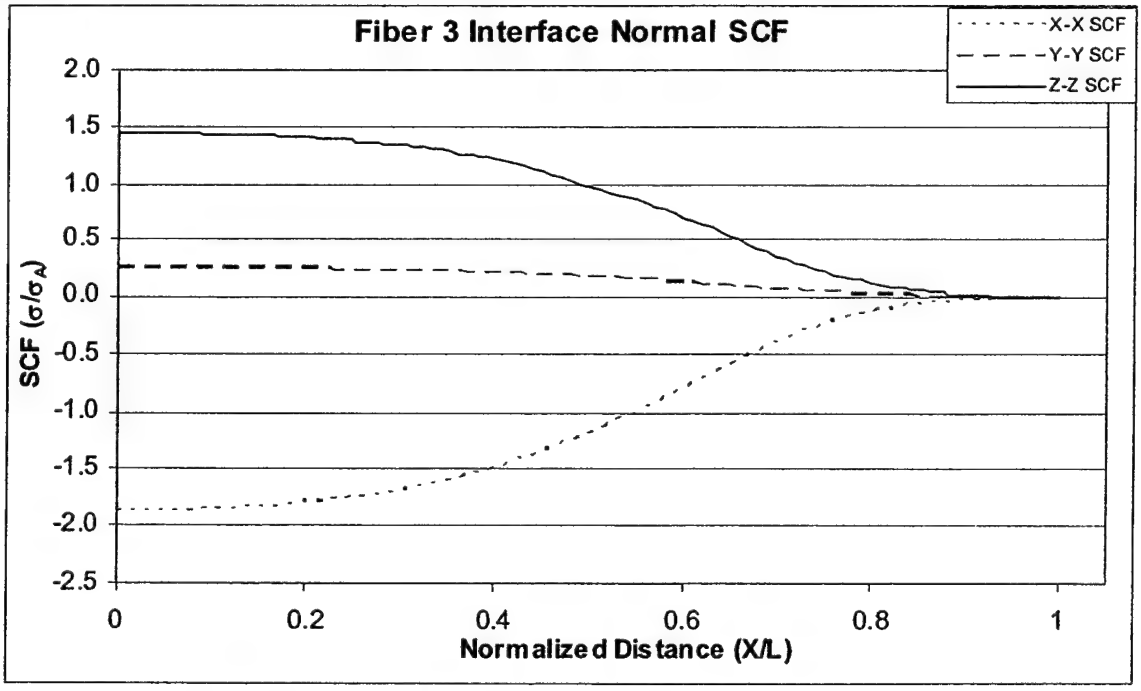

Figure 13. Normal SCFs at the fiber/matrix interface for Fiber 3.

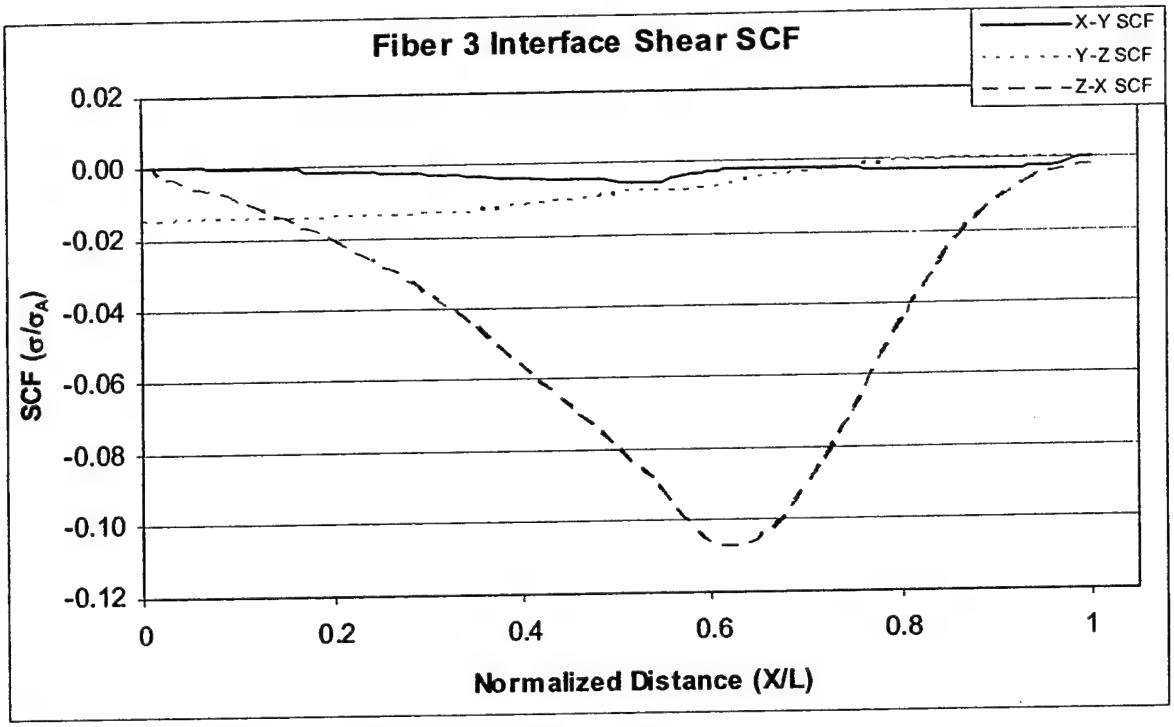

Figure 14. Shear SCFs at the fiber/matrix interface for Fiber 3.

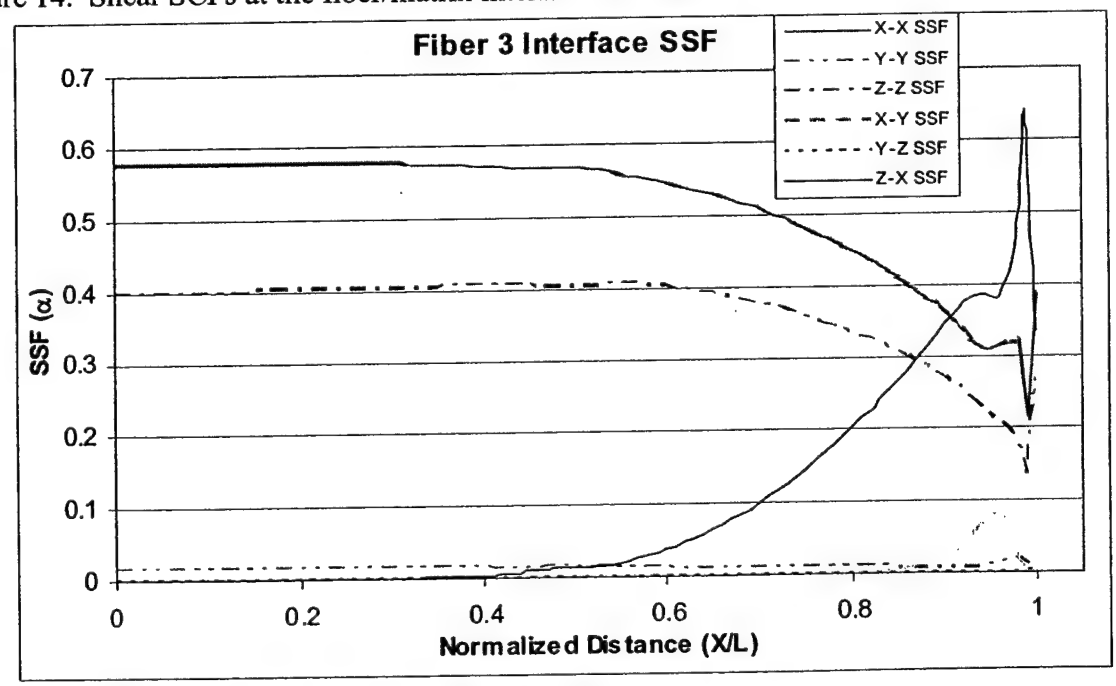

Figure 15. SSFs at the fiber/matrix interface for Fiber 3.

First RVE 9-Fiber Model These fibers are quite small, and as a consequence, the aspect ratios of the elements become much greater, up to a value of 17. The number of elements has risen to 199,440. Aspect ratios this high and the number of elements required serve as proof that a RVE approach has become a necessity.

9-Fiber Stress concentration factors Fiber 4 experienced the highest transverse stress, while fiber 1 experienced the least. Transverse SCFs for these two fibers are shown in Figure 16. Fiber 4 had an intermediate axial SCF, between the maximum in fiber 1 and the minimum in Fiber 9, will be used for comparison with single fiber and four fiber analyses. Normal and shear SCF from fiber 4 are plotted in Figures 17 and 18, respectively. Stress sensitivity factors for fiber 4 are presented in Figures 19.

As was the case with the four-fiber model, all the SCF curves are similar in shape to the single fiber model. Looking at the minimum and maximum transverse SCF, a 5.5% difference was found at (X = 0). Axial SCF at the center of fibers 1 and 9 remain close in the central region. However, as the wing tip is approached (X/L > 0.83), fiber 1 starts to experience a positive axial stress; fibers 4 and 7 do as well. The magnitude of these stresses is low (1.16 MPa – fiber 1) relative to the compressive stress seen in the rest of the fiber. Normal and shear SCF of fiber 4 are very similar to those of the single fiber model and fiber 3 in the four-fiber model. The Z-X shear SCF has a maximum magnitude of -0.155 at X/L = 0.62.

9-Fiber Stress sensitivity factors Again, as one would expect, transverse and axial stresses contribute most to the von Mises in the specimen's central region (Figure 19). At a normalized distance greater than 0.77 the Z-X shear becomes completely dominant up to 0.94 where X-Y shear takes over. This behavior was not seen in previous models. Thus, as more fibers are added to the model, the stress field near the wing tip becomes more complicated.

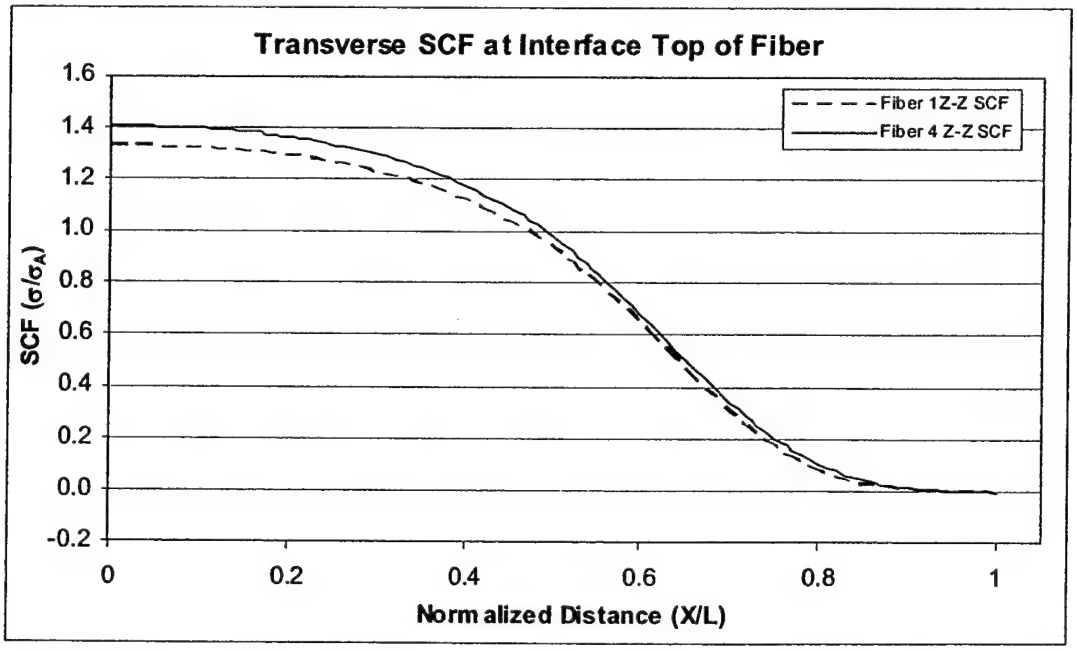

Figure 16. Comparison of interfacial transverse SCFs for the two of the nine fibers.

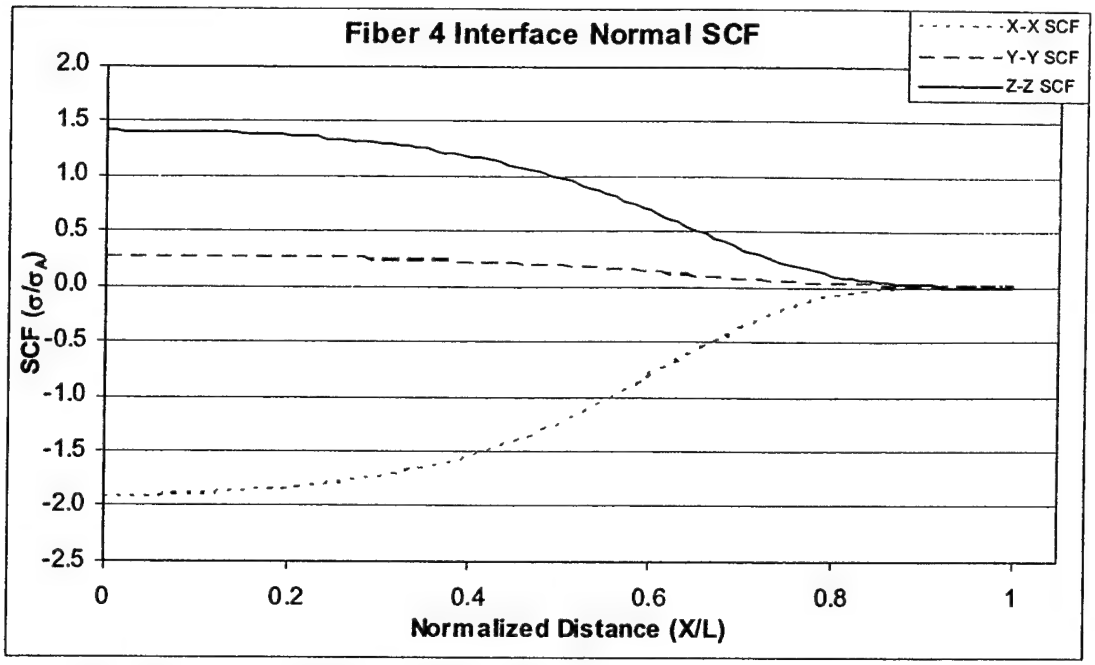

Figure 17. Interfacial normal SCFs for fiber four.

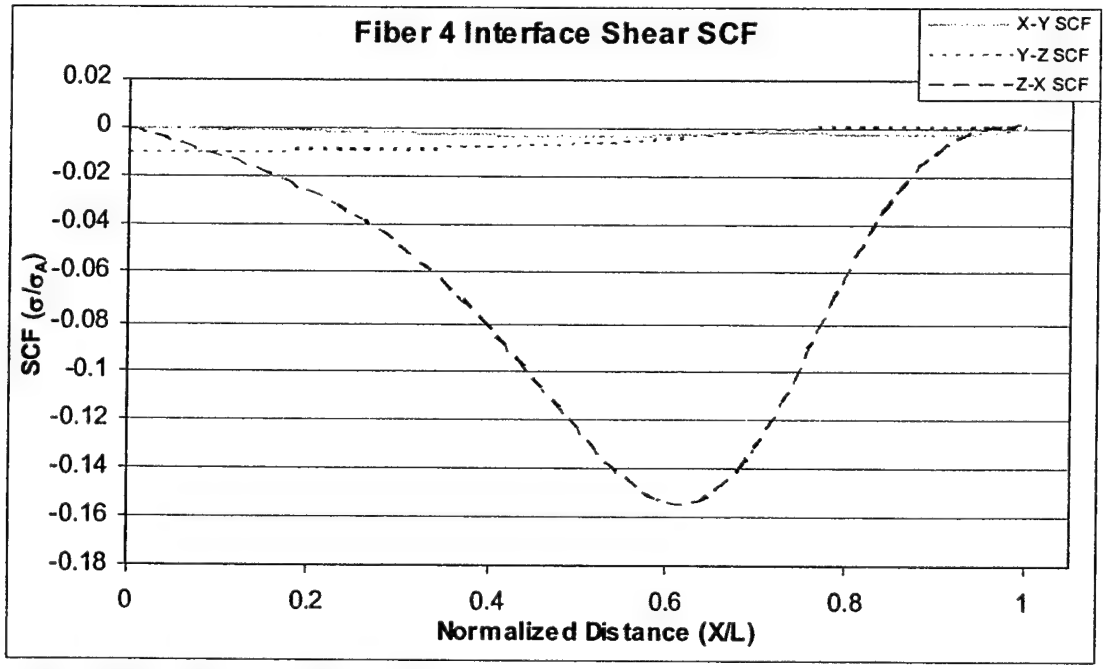

Figure 18. Interfacial shear SCFs for fiber four.

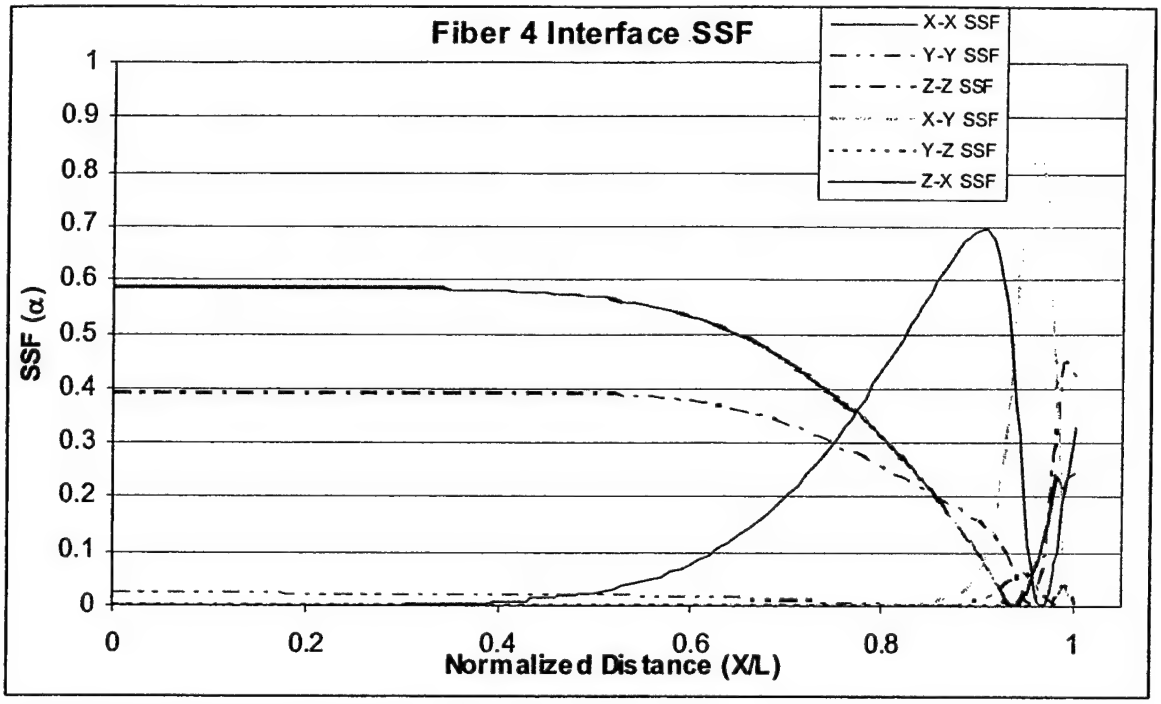

Figure 19. Stress sensitivity factors for fiber four.

First RVE Model Comparisons Transverse SCF from the single fiber model are plotted with the SCF from the representative fibers of the four and nine fiber models in Figure 20. Likewise, the Z-X shear SCF are shown in Figure 21. All three models exhibited similar transverse stress behavior through the model's width. However, there is a significant difference in the maximum values at the specimen center. The single fiber model resulted in a maximum transverse stress of 32.48 MPa, while fiber 3 in the four-fiber model experienced 36.25 MPa. This is a difference of 10.4%, but looking back to the four-fiber model analysis, fiber 1 experienced 7% less transverse stress than fiber 3. Thus, fiber 1 of the four-fiber model produced transverse stress results more similar to the single fiber model.

Analysis of the single fiber model resulted in a maximum Z-X shear of -5.16 MPa at X/L = 0.61. Fiber 3 of the four fiber model showed a maximum Z-X shear of -2.69 MPa at X/L = 0.62. These stresses are relatively low when compared to the maximum transverse stresses (~35 MPa). The importance of these shear stresses depends on the system's interfacial shear strength relative to the interfacial transverse strength.

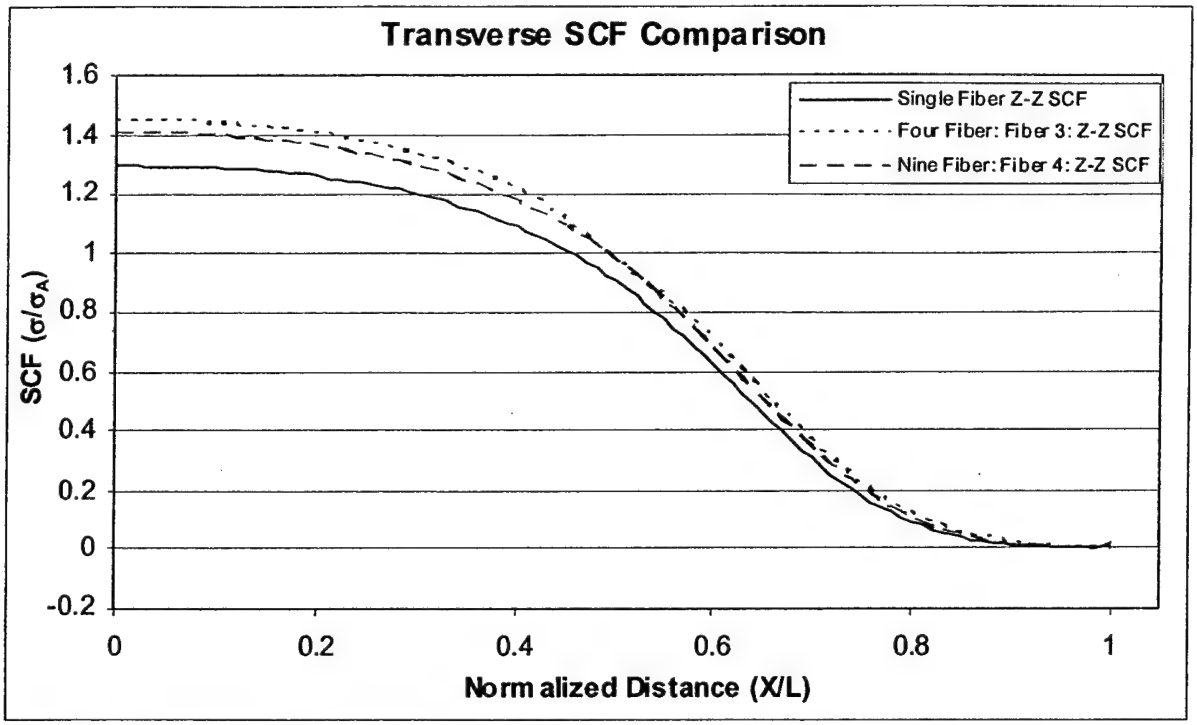

Figure 20. Transverse SCF comparison for 1, 4 and 9-fiber models.

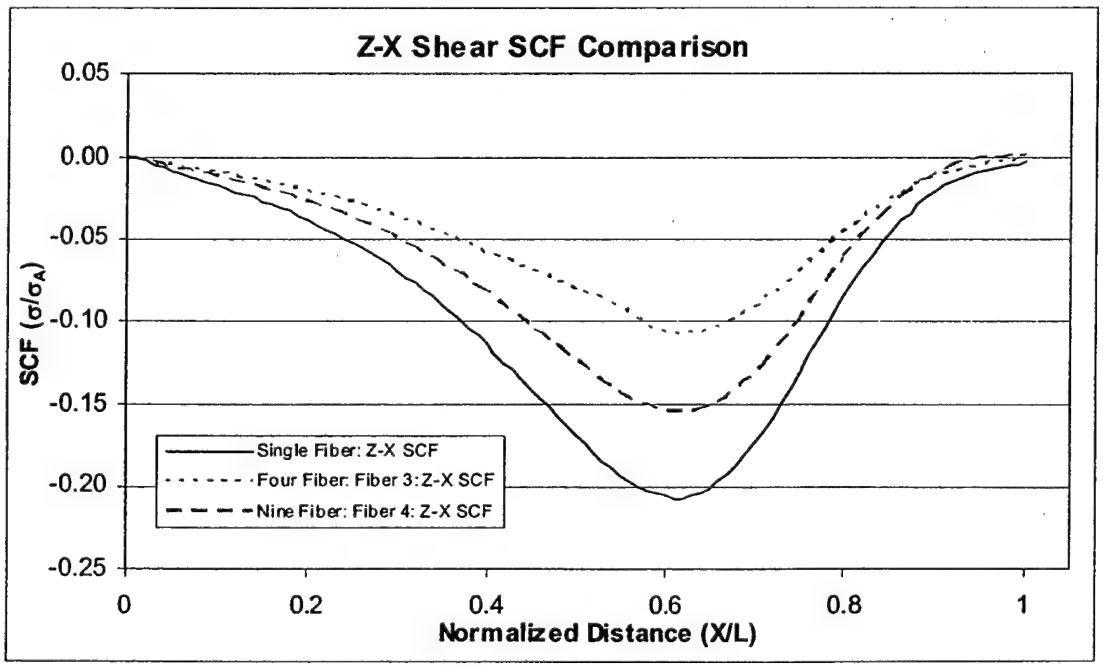

Figure 21. Shear SCF comparison for 1, 4 and 9-fiber models.

Second RVE Model For the second RVE model, models similar to the first model were utilized except in this case the fiber radius was chosen such that the total fiber cross-sectional area was equivalent to the cross-sectional area of 125 of the 27 μm diameter optical fibers used in the optical fiber sensor system that is the subject of this grant. Tables 4-6 contain the cruciform

specimen geometry (Table 4), the material properties used (Table 5) and the model parameters (Table 6). The mesh used for finite element analysis of the ¼, 1 and 4 fiber second RVE models are shown in Figures 22-24. These figures show the biasing used to limit the number of elements and the aspect ratios for the elements. The stress concentration factor and stress sensitivity factor curves all exhibited similar behavior to those in the first RVE model section, only the magnitudes are different.

Table 4: Dimensions of the second RVE cruciform specimen to be modeled

Parameter	2A	2H	2L	T	R	2G
Value	10 mm	2.32 mm	18.88 mm	4 mm	4.29 mm	15 mm

Table 5: Material properties and load for the second RVE model

Constituent	Young's Modulus	Poisson's Ratio	σ_A(Applied Stress)
Matrix	3.4 GPa	0.35	25 MPa or N/mm^2
Fiber	55 GPa	0.20	

Table 6: RVE fiber diameters, number of elements and largest aspect ratios for the second RVE model

Model Name	Fiber Diameter	Number of Elements	Largest Aspect Ratio
Quarter Fiber	0.3018 mm	79940	3.6
Single Fiber	0.151 mm	128880	8.7
Four Fiber	0.0755 mm	176440	17

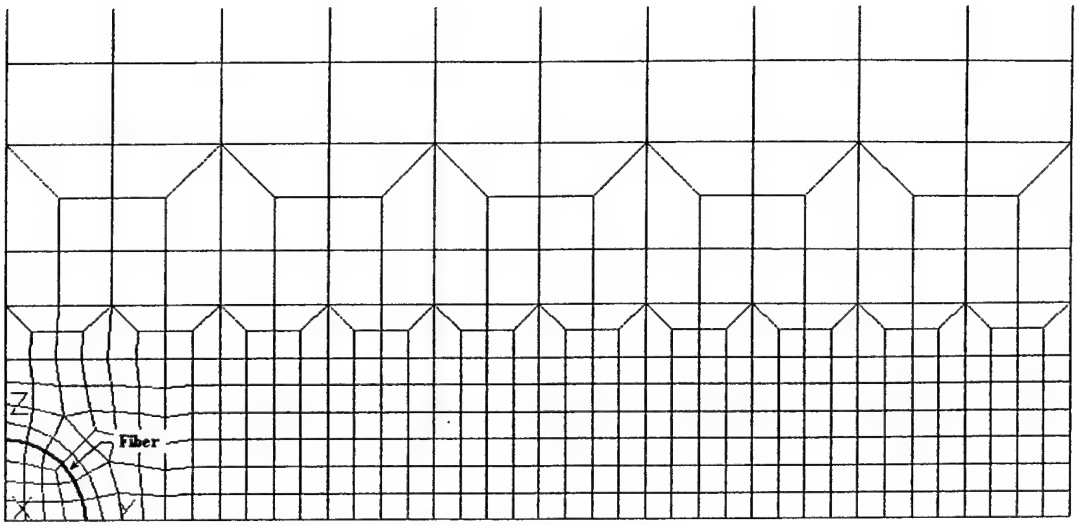

Figure 22. Finite element analysis mesh for ¼ fiber model.

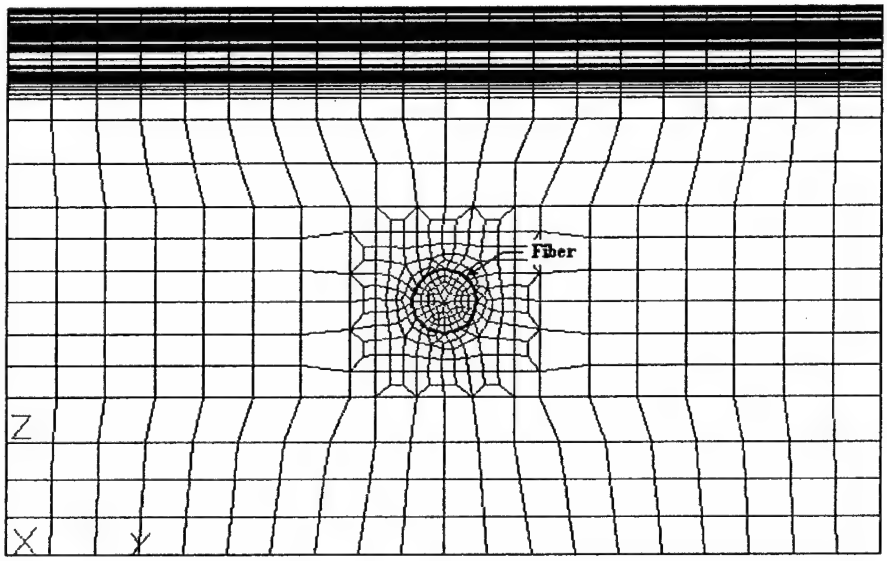

Figure 23. Finite element analysis mesh for 1-fiber model.

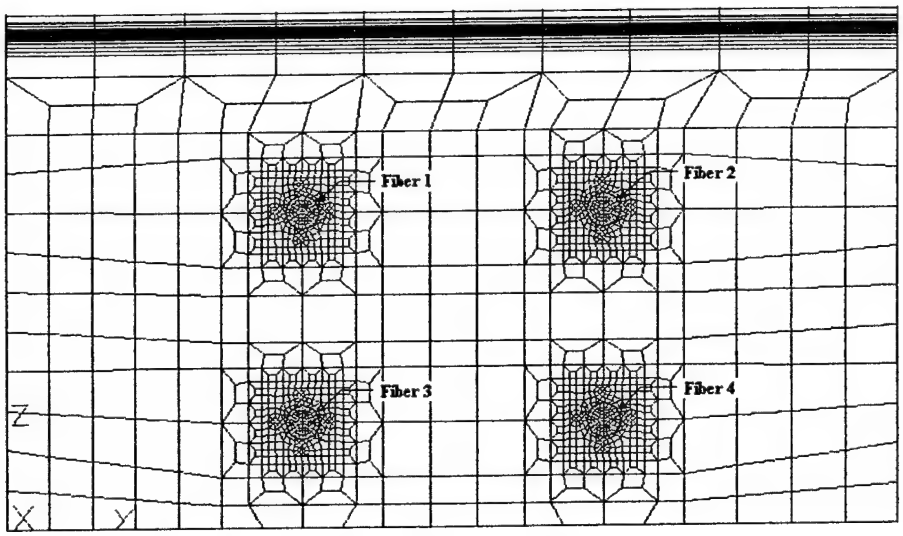

Figure 24. Finite element analysis mesh for 4-fiber model.

Second RVE Model – Transverse SCFs Fiber 3 (Figure 24) of the four-fiber model was chosen for comparison. The ¼ fiber model resulted in slightly lower transverse stress at the interface, as shown in Figure 25. Because fiber 3 in the four-fiber model experienced the highest stresses while the quarter fiber experienced the least, these two were used for comparison. There is a 3.6% difference between the maximum transverse stress of 36.7 MPa found at the interface of fiber 3 in the four fiber model and the maximum of 35.4 MPa found in the quarter fiber model. To gain a more complete understanding of the difference in these two models the m-estimator technique was applied to the fractional difference $(\sigma_A-\sigma_B)/\sigma_A$ in the stresses along the entire fiber length. From the data shown in Figure 25, the largest visual differences occur in the central portion of the specimen. The red lines show the beginning and end of the wing fillet. Thus, prior to the beginning of the wing (red line at ~0.5), larger differences are seen. However, in the wing area the percent difference can exceed 100%, due to the small value for σ_A. The m-estimator technique is designed to reduce the contribution of these outlying values. M-estimation resulted in an average difference of 6.0% along the fiber length, complementing the difference at the maximum value of 3.6%.

Second RVE Model – Axial SCFs The axial SCF from the quarter fiber model behaves slightly differently than the other axial SCFs and does not approach zero as rapidly. This may be due to boundary conditions being applied at the fiber's center nodes, which do not allow the fiber to displace in the Z direction. Also, in the center section, the ¼ fiber model has the lowest axial SCF, while the 4-fiber model has the greatest axial SCF. In the wing section the situation is reversed. The maximum axial stress of -175.7 MPa was found in fiber 3 of the four-fiber model; again there is a 3.5% difference between this value and the maximum of -169.6 MPa found in the ¼ fiber model. These axial SCFs are 4.5-5 times the maximum transverse SCFs. M-estimator analysis led to an average 9.8% difference between the axial stress experienced by fiber 3 and the quarter fiber.

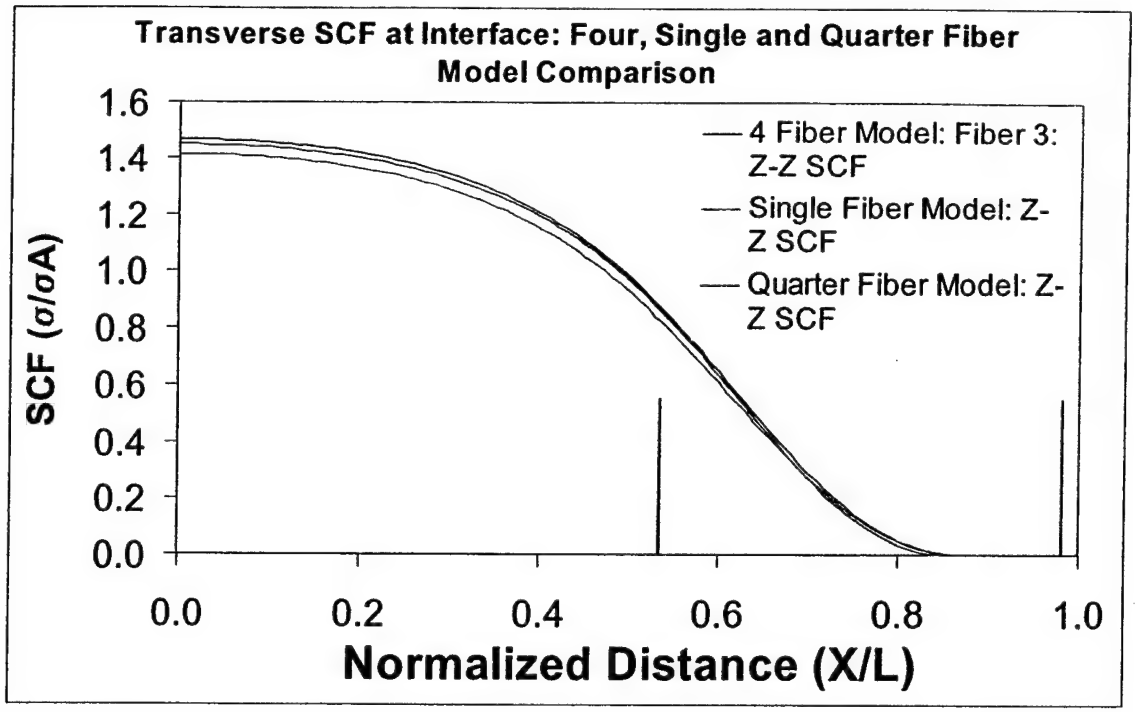

Figure 25. Comparison of transverse SCFs for the second RVE model system.

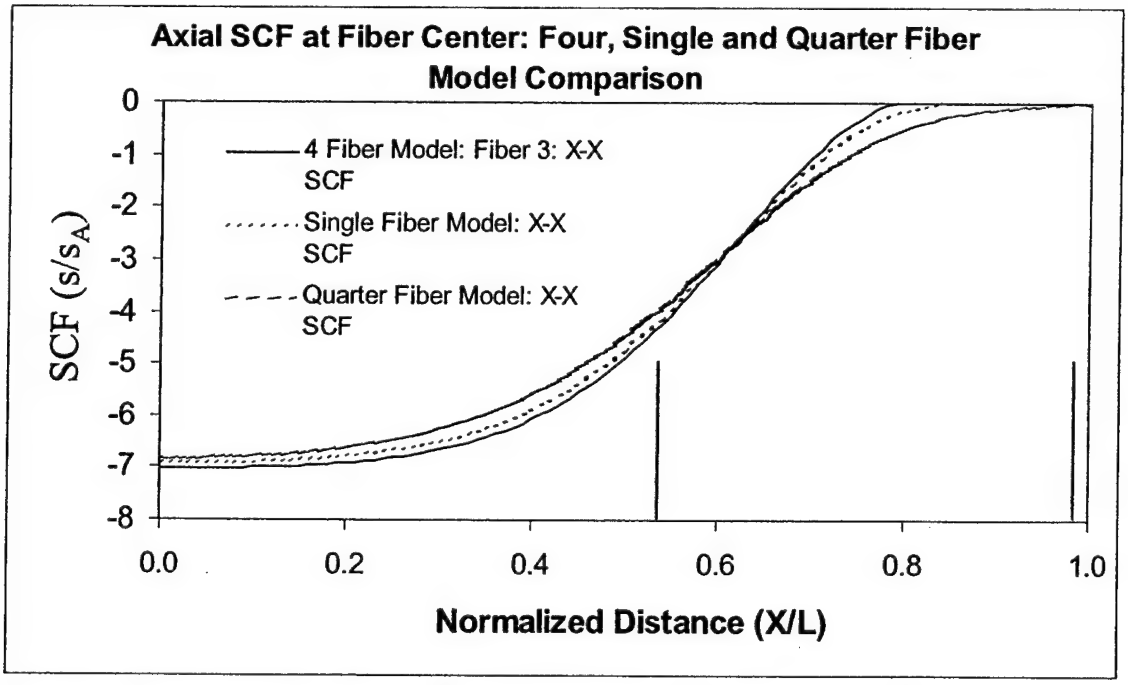

Figure 26. Comparison of axial SCFs for the second RVE model system.

Second RVE Model – SSFs Figure 27 shows the stress sensitivity factors (SSFs) found for the single fiber second RVE model. The ¼ and 4-fiber models show SSFs very similar to this figure and are therefore not shown. In Figure 27, the axial X-X stress is the dominant stress within the central section (X/L < ~0.52), with the transverse stress also relatively large, as the von Mises

stress begins to decrease in the wing region, the shear stresses become much more important. This behavior was expected; however, the large axial stress seen in both RVE models makes use of the cruciform test to generate transverse stresses and calibrate our fiber-optic sensor system problematic. To examine conditions that might ameliorate this situation, simulations were performed with a variety of alternate material property values.

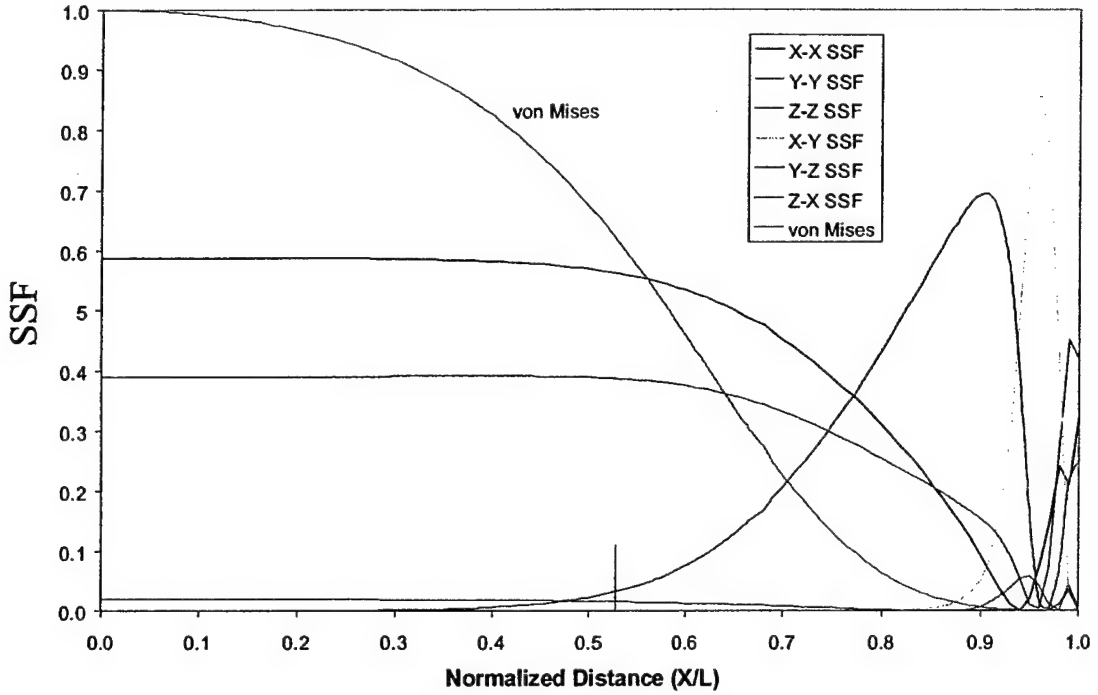

Figure 27. Stress sensitivity factors (SSF) for the single fiber second RVE model.

Alternate Material Property Simulations

Additional single fiber models were analyzed to investigate the effect of changing Young's modulus and/or Poisson's ratio. To make the fiber and matrix properties more similar, the matrix Young's modulus was doubled, while the fiber's was halved; the matrix Poisson's ratio was reduced by 0.03 and the fiber's increased by 0.03. This is designated as alternate materials comparison (AMC) 1 with the material properties shown in Table 7. In AMC 2, the Young's moduli and Poisson's ratios for both constituents were equated at the average value of the fiber and matrix. AMC 3 was designed with equal Poisson's ratios again at the fiber/matrix average and the original Young's moduli of the fiber and matrix. The fourth analysis (AMC 4) was carried out with equal Young's modulus and original Poisson's ratios. Material properties used in all the comparison models are presented in Table 7. The transverse and axial SCFs for AMC 1, AMC 2 and the original specimen, are plotted in Figures 28 and 29, respectively. When the material properties became slightly more similar (AMC 1), there was a reduction of 9.5% in the maximum transverse stress seen at the fiber/matrix interface, as shown in Figure 28. However, Figure 29 shows a reduction of 78.8% in the maximum axial stress experienced by the fiber. As transverse loads are the point of interest and fiber compression was a concern, the large reduction

in axial stress compared to transverse stress is desirable. When the properties were set equal (AMC 2), transverse stress dropped below the applied stress (Figure 28) and the axial stress dropped to almost zero (Figure 29). Equal Poisson's ratios (AMC 3) led to only a slight reduction in the maximum transverse stress (2.1%), while equal Young's modulus (AMC 4) resulted in a reduction of 33.8%, as seen in Figure 30. Figure 31 shows the 16.4% drop in maximum fiber axial stress when Poisson's ratios are equal (AMC 3), but there is a 95.8% drop for equal Young's modulus. Results from the equal Young's modulus and equal Poisson's ratio models show that Young's modulus differences have a greater effect on the system. Thus, the cruciform test may become usable for testing the fiber-optic sensing system, when the matrix Young's modulus is increased. This may be accomplished by filling the matrix with stiff nanoparticles or by utilizing unidirectional composite materials rather than pure polymer.

Table 7: Material properties used in comparison models

Model	Constituent	Young's Modulus	Poisson's Ratio
AMC 1	Matrix	6.8 GPa	0.32
	Fiber	27.5 GPa	0.23
AMC 2	Matrix	29.2 GPa	0.28
	Fiber	29.2 GPa	0.28
AMC 3	Matrix	3.4 GPa	0.28
	Fiber	55 GPa	0.28
AMC 4	Matrix	29.2 GPa	0.35
	Fiber	29.2 GPa	0.20

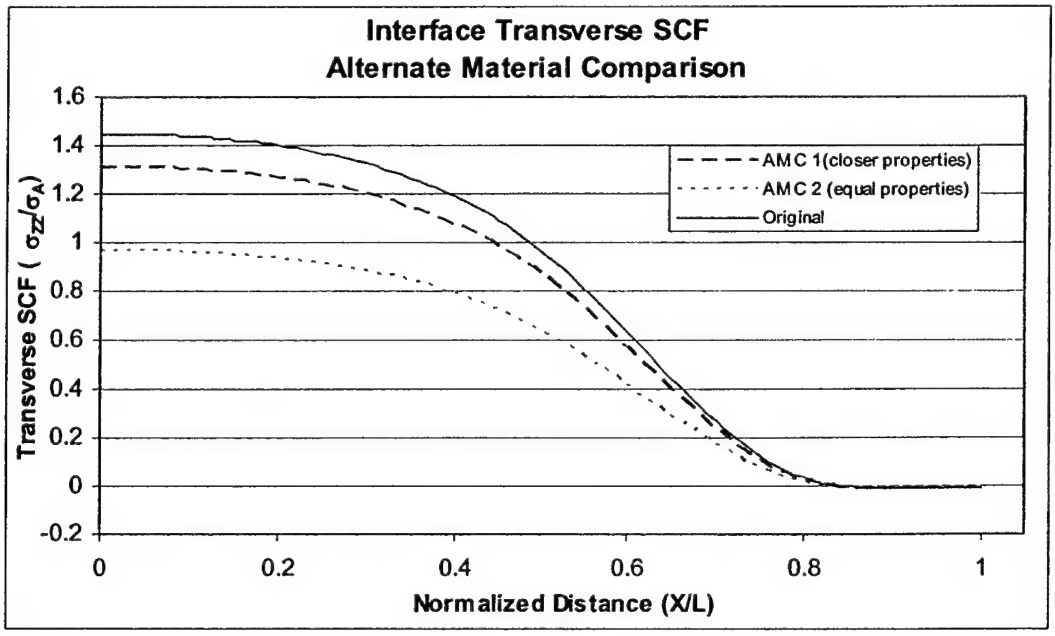

Figure 28. Comparison of transverse SCFs for AMC1, AMC2 and original model.

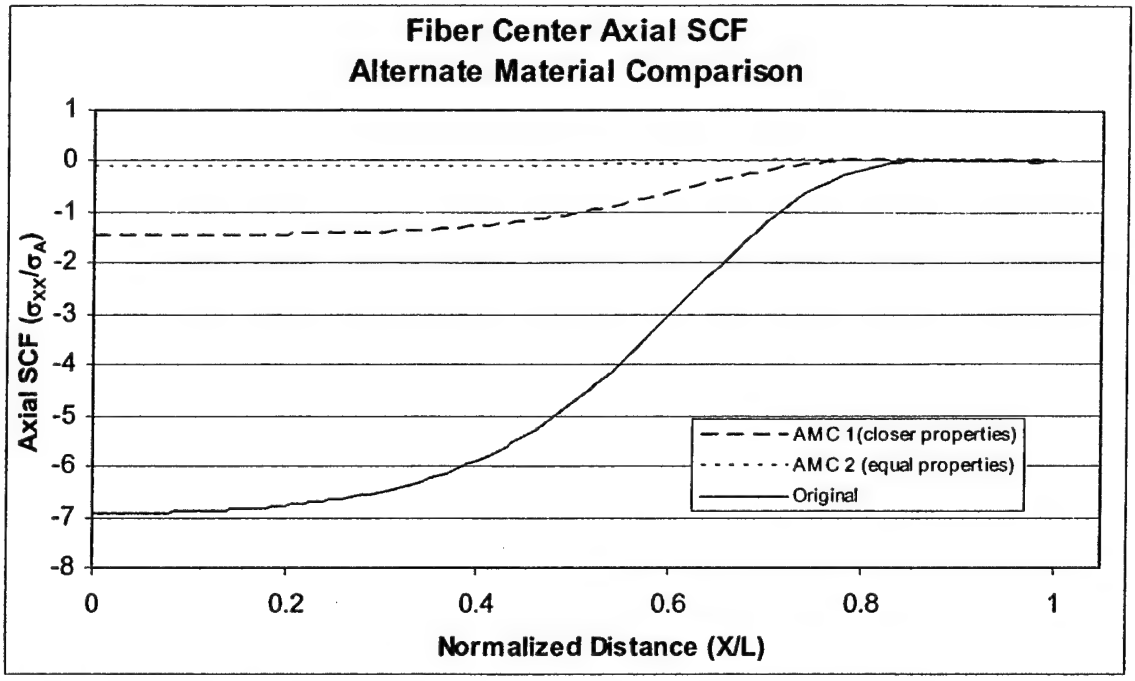

Figure 29. Comparison of axial SCFs for AMC1, AMC2 and original model.

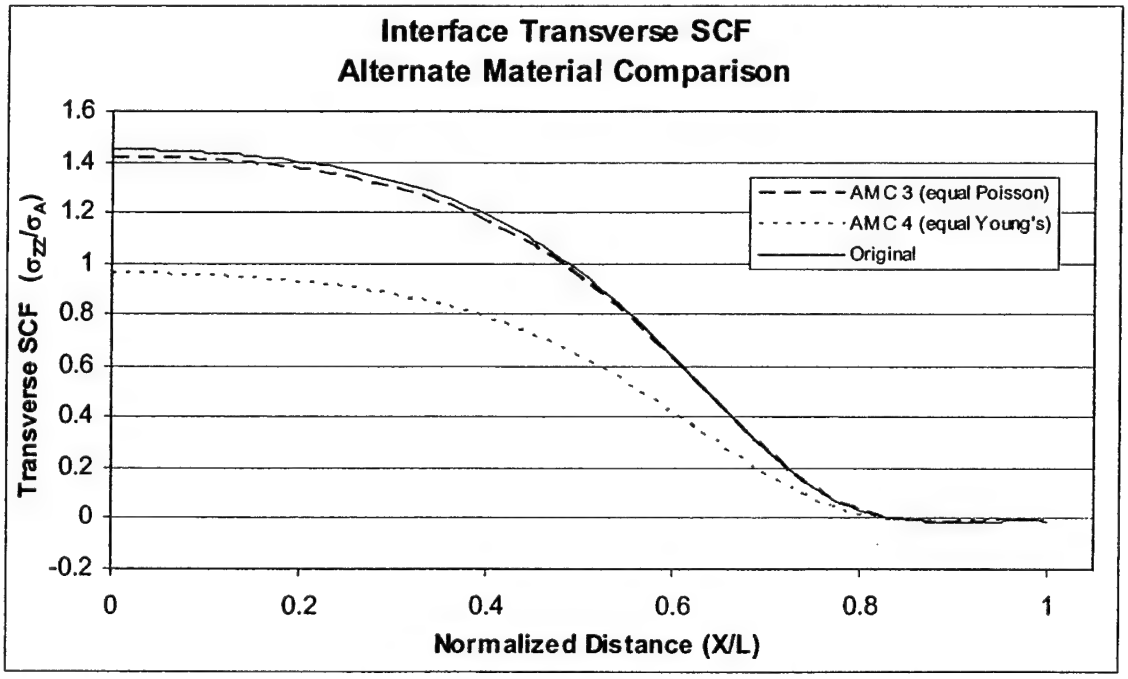

Figure 30. Comparison of transverse SCFs for AMC3, AMC4 and original model.

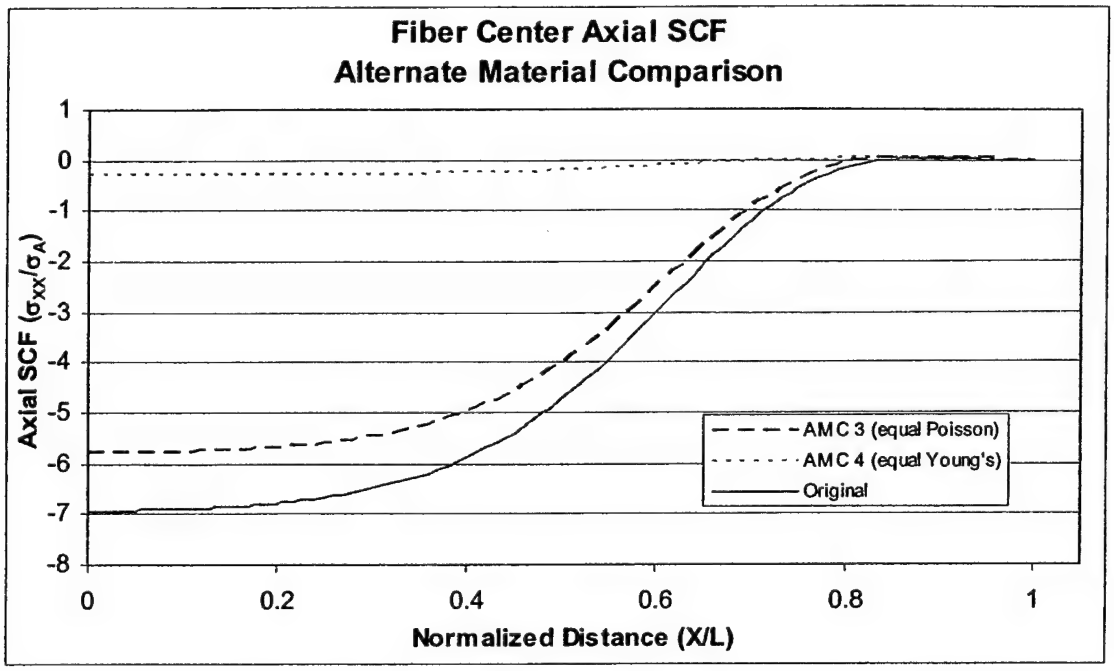

Figure 31. Comparison of axial SCFs for AMC3, AMC4 and original model.

D. Future Work

This reporting period marks the end of this research grant. Due to availability issues, a portable spectrometer card for examining, *in situ*, a system of importance to the Air Force could not be obtained prior to the expiration of this grant. Therefore, this work will be performed after the grant completion and included in the final report.

5. PERSONNEL SUPPORTED:

Faculty:

Dr. Jon J. Kellar, Department of Materials and Metallurgical Engineering
Dr. Lidvin Kjerengtroen, Department of Mechanical Engineering

Research Scientist:

Dr. William M. Cross, Materials Engineering and Science Program

Graduate Students:

Mr. Wayne Weyer, Mechanical Engineering Department
Mr. Robert Pentland, Materials Engineering and Science Program

6. PUBLICATIONS:

1. W. Weyer, W. Cross, J Kellar and L. Kjerentroen, "Finite element evaluation of a unidirectional, transversally loaded, multi-fiber cruciform test specimen: Employing representative volume element theory," in review, **Composites Science and Technology**.

7. INTERACTIONS/TRANSITIONS:

a. Participation/Presentations at Meeting, Conferences, Seminars etc.

1. L. Kjerengtroen, J. Kellar, W. Cross, K. Coleman, R. Pentland and W. Weyer, "Total Lifetime Health Monitoring System for Polymer Matrix Composites," ASME 2003 Mechanics and Materials Conference, June, 2003, Scottsdale, AZ.

b. Consultative and Advisor Functions.

A bond line application was attempted but due to a failure of the light source of the spectrograph card (Control Development, New Castle IN) utilized, no relevant research data could be collected.

c. Transitions.

The patented fiber-optic sensing system for polymer matrix composites has been transitioned to grant F29601-02-C-0245, "Improved Performance of Composite Tanks in Cryogenic Storage Applications" a small business technology transfer grant through the Air Force Research Laboratory, Space Vehicle Division, Kirtland Air Base, NM.

8. NEW DISCOVERIES, INVENTIONS, OR PATENT DISCLOSURES:

Nothing yet to report.